Journal of *Marine Science and Engineering*

MDPI

Article

A Consolidated Linearised Progressive Flooding Simulation Method for Onboard Decision Support

Luca Braidotti [1,*], Jasna Prpić-Oršić [2], Serena Bertagna [1] and Vittorio Bucci [1]

[1] Department of Engineering and Architecture, University of Trieste, via Valerio 10, 34127 Trieste, Italy; sbertagna@units.it (S.B.); vbucci@units.it (V.B.)
[2] Faculty of Engineering, University of Rijeka, Vukovarska 58, 51000 Rijeka, Croatia; jasnapo@riteh.hr
* Correspondence: lbraidotti@units.it

Abstract: In pursuing quick and precise progressive flooding simulations for decision-making support, the linearised method has emerged and undergone refinement in recent years, becoming a reliable tool, especially for onboard decision support. This study consolidates and enhances the modelling approach based on a system of differential-algebraic equations capable of accommodating compartments filled with floodwater. The system can be linearised to permit analytical solutions, facilitating the utilization of larger time increments compared to conventional solvers for differential equations. Performance enhancements are achieved through the implementation of an adaptive time-step mechanism during the integration process. Furthermore, here, a correction coefficient for opening areas is introduced to enable the accurate modelling of free outflow scenarios, thereby mitigating issues associated with the assumption of deeply submerged openings used in governing equations. Experimental validation is conducted to compare the method's efficacy against recent model-scale tests, specifically emphasising the improvements stemming from the correction for free outflow.

Keywords: damaged ship; progressive flooding; linearised method; free outflow; decision support; experimental test; decision support

Citation: Braidotti, L.; Prpić-Oršić, J.; Bertagna, S.; Bucci, V. A Consolidated Linearised Progressive Flooding Simulation Method for Onboard Decision Support. *J. Mar. Sci. Eng.* **2024**, *12*, 1367. https://doi.org/10.3390/jmse12081367

Academic Editor: Valery M. Abramov

Received: 10 July 2024
Revised: 5 August 2024
Accepted: 9 August 2024
Published: 11 August 2024

1. Introduction

Decision Support Systems (DSSs) have recently emerged as a promising application field for progressive flooding simulations, providing crucial assistance to crews in operational environments [1]. This is particularly significant for large passenger ships, which carry thousands of people and are susceptible to flooding accidents due to their complex subdivision, limited stability, and reduced freeboard at the bulkhead deck [2]. Predicting the behaviour and final fate of a damaged ship in real time is vital for ensuring the safety of passengers and crew, a task that is challenging without a DSS. Traditionally, decision support relies on static means such as mandatory booklets or loading computers, which cannot provide any insight into the transient and progressive flooding phases [3]. Recent advancements have integrated progressive flooding simulations into onboard DSSs, greatly enhancing their ability to quickly and accurately assess situations and make informed decisions during emergencies. These systems employ progressive flooding simulations directly onboard, relying on flooding sensors [4–6] or leverage extensive datasets of progressive flooding simulations [7–11].

Quasi-static methods are preferred for simulating progressive flooding within DSSs due to their good balance between speed and accuracy compared to fully dynamic codes [12,13] and Computational Fluid Dynamics (CFD) tools [14–16]. These methods assume a horizontal and flat free surface within flooded compartments, utilizing hydraulic laws (typically the Bernoulli equation) to model flow behaviour through openings. While early quasi-static methods were based on empirical formulations [17], more advanced techniques have

been developed to manage complex ship subdivisions and asymmetric flooding scenarios [18,19]. These improvements include accounting for air compression effects through pressure correction [20–22], employing predictor–corrector schemes to solve nonlinear systems for internal pressures [23,24], using adaptive meshes for pressure integration [25], and implementing dynamic orifice equations instead of the Bernoulli one [26,27].

Few simulation tools have been designed for direct onboard applications. First, a method based on flooding chains was proposed in [28], which simplifies calculations by ignoring air compression and dynamic effects to achieve faster results. Although this approach significantly compromises accuracy, it was deemed sufficient for real-time decision support as it qualitatively replicates the flooding process with large time steps [29]. The pressure correction technique has also been updated to reduce computational effort through variable time steps [30]. Finally, a method for onboard application based on the linearisation of governing equations has been introduced, improved with adaptive time steps [31], and tested on a full-scale cruise ship [32]. The key assumption to enabling linearisation is that the flow at openings is deeply submerged. However, this simplification may not be accurate enough in all scenarios. Real ship environments often encounter free outflow situations, where floodwater does not fully submerge openings between compartments.

The main novelty of the paper is the introduction of an updated formulation that includes corrections for free outflow to overcome these limitations inherent in the previous method. This involves adjusting the effective area of openings to account for free outflow, thereby improving the accuracy of simulations without increasing computational complexity. The paper validates the updated formulation against experimental tests available in the literature and provides a detailed analysis by comparing the simulation results with experimental data from a challenging test case. This comprehensive analysis will highlight the strengths and weaknesses of linearised techniques and guide future work needed to support its direct onboard application for decision support after damage.

The remainder of the paper is organized as follows. Section 2 presents the consolidated simulation technique with a focus on free outflow modelling. Section 3 validates the updated methodology with free outflow correction. Section 4 compares the consolidated simulation results with experimental results for a cruise ship model. Section 5 discusses the results, leading to the conclusions in Section 6.

2. Materials and Methods

This section presents the linearized solution to the progressive flooding problem, derived from the conservation of mass and momentum equations under the assumption of deeply submerged flow at openings. The proposed method for modelling free outflow cases within this linearized framework is also discussed. This study, based on the state-of-the-art methodology by [31], introduces the main assumptions of the progressive flooding simulation technique, providing a consolidated version of the method in order to foster its applicability in an operative environment. The method is implemented using custom-built software coded in Java.

2.1. Assumptions and Reference Systems

The simulation operates under quasi-static conditions, excluding dynamic phenomena other than floodwater transfer. The sea's free surface and waterplanes within flooded compartments are assumed to be flat and parallel to the sea's free surface. Two coordinate systems are defined (Figure 1): the ship-fixed right-handed system $OXYZ$ with its origin at the baseline and aft perpendicular, and the auxiliary Earth-fixed right-handed system $O'xyz$ corresponding to the sea's free surface, where waterplanes in flooded compartments are identified by a level z. This auxiliary system is updated at each time step based on the vessel's floating position, determined by the initial loading condition and accumulated floodwater.

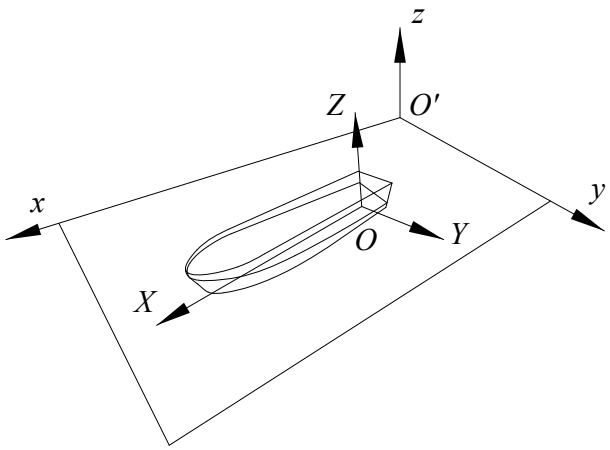

Figure 1. Ship-fixed and auxiliary Earth-fixed reference systems [31].

All internal spaces are assumed to be fully ventilated to foster the application in an operative environment. Air compression is significant only in rooms connected by small vent openings, such as tanks with ventilation pipes [20] or in airtight rooms where stable air pockets may form when all openings are submerged. Typically, 3D ship models for stability assessments do not include these details. Additionally, uncertainties in the ship model (e.g., permeabilities, opening sizes, and discharge coefficients) can affect simulation reliability [33], reducing the benefits of modelling air compression.

Finally, to facilitate the solution of the linearised system of equations, it is assumed that all openings are deeply submerged, meaning the upper tip of each opening is below the water level in both connected spaces. However, free outflow scenarios, where openings are partially submerged at least on one side, can occur due to side damage or during the initial flooding of a new room. This assumption may introduce significant errors in progressive flooding simulations, as will be demonstrated and discussed later. To address these concerns, this study proposes a correction to model free outflow cases as deeply submerged by modifying the effective area of the opening, which is assumed to have a rectangular shape.

2.2. Main Calculation Loop

The primary iterative loop of the simulation procedure, illustrated in Figure 2, involves several key steps. Initially, the vessel's displacement and centre of mass are determined to assess its floating state [34]. If a feasible equilibrium is not achieved, the vessel will sink or capsize, terminating the simulation. Otherwise, new water levels $\mathbf{z}^*$ within the flooded compartments are calculated to conserve the floodwater volume.

The submerged areas of all openings, connecting two flooded compartments or a flooded compartment to an empty one (referred to as Progressive Flooding Openings, PFOs), are then evaluated. If the openings are deeply submerged, the submerged area equals the opening area and requires no adjustment. Otherwise, free outflow occurs, and areas equivalent to the deeply submerged scenario are calculated and applied to the openings experiencing free outflow.

If any PFO has a non-zero submerged area, a new flooded compartment is considered in the simulation. Complex internal layouts may cause counterflows, potentially draining previously flooded compartments or surfacing previously submerged openings. Thus, the status of the connections between flooded compartments must be verified, moving surfaced connections to the PFO list and removing emptied compartments. In certain cases, floodwater may be trapped by the surfacing of all connections, and such compartments are treated as tanks in the subsequent equilibrium assessment.

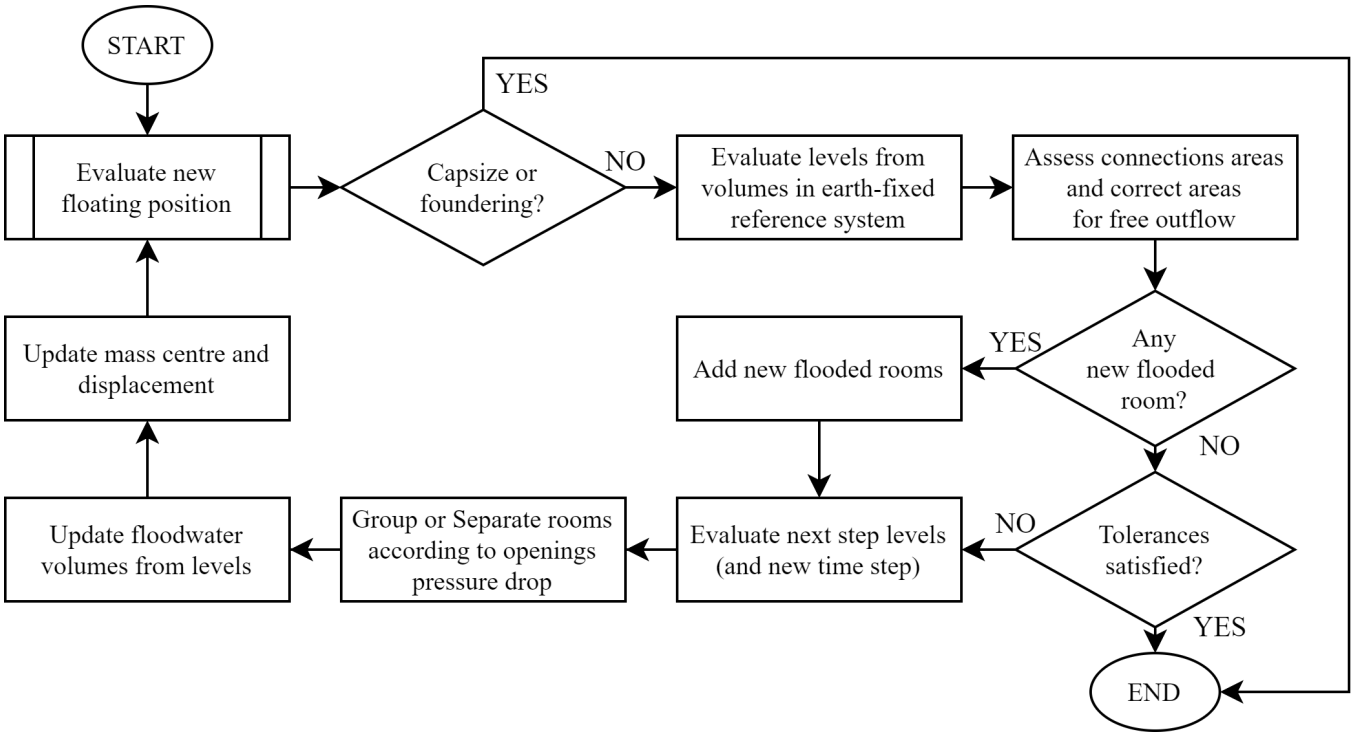

Figure 2. Flowchart of the main loop of the simulation process

If no new flooded compartments are detected, the floating position and floodwater levels are checked to determine if the vessel has reached a new stable floating position. Two convergence conditions must be met: the rate of change of the heel angle ϕ, the trim angle θ, and the mean draught T_M must be within limits, and the water level inside non-fully flooded compartments must correspond to the flat sea surface, i.e., shall be null in the Earth-fixed reference system. Table 1 outlines the tolerances for these criteria, where distances are normalised with the initial mean draught of the ship T_{M_0}. If the convergence criteria are not satisfied, the water levels for the subsequent time increment are recalculated using the explicit solution of linearized differential equations for partially filled rooms and by solving a nonlinear system for fully flooded rooms.

Table 1. Applied thresholds of the stopping algorithm and grouping/separation

Description	Bounded Value	Threshold
Heel Angle	$\lvert\phi_n - \phi_{n-1}\rvert/\mathrm{d}t$	0.00050 deg/s
Trim Angle	$\lvert\theta_n - \theta_{n-1}\rvert/\mathrm{d}t$	0.00005 deg/s
Mean Draught	$\lvert T_{M_n} - T_{M_{n-1}}\rvert/(T_{M_0}\mathrm{d}t)$	0.00001 1/s
Level	$\lvert z_i\rvert/T_{M_0}$	0.0001
Grouping	$\lvert z_i\rvert/T_{M_0}$	0.0005

As the flow rate through openings decreases, the pressure drop across the openings becomes negligible, resulting in the equalization of water levels between interconnected rooms or between a room and the sea. This equalization renders the equation system unsolvable [31], prompting flooded rooms with similar levels to be aggregated into a fictitious room, thereby reducing the system's rank. The threshold for grouping is specified in Table 1. The water level z_f of the grouped rooms is given by

$$z_f = \frac{S_i z_i + S_j z_j}{S_i + S_j} \tag{1}$$

where z_i and z_j are the water levels of the rooms and S_i and S_j are their free surface areas. If one room represents the sea, a zero level is imposed on the group. If one room is fully flooded, the water level of the other room is imposed on the group. During each iteration, the flux through openings connecting grouped rooms is examined to ensure the conservation of mass. If the velocity introduces a pressure drop exceeding the grouping threshold, the rooms are separated, imposing a level difference equal to the pressure drop. This procedure prevents computational errors that may arise from accelerated flow, such as during sudden heeling or the collapse of a closed non-watertight opening.

Subsequently, the volumes of water within the flooded rooms for the next time step are computed based on the updated water levels, establishing a new loading condition to initiate another iteration of the main computational loop.

2.3. Governing Equations

In the Earth-fixed reference system with its origin at the sea's free surface and a vertical axis z orthogonal to the surface (positive upwards), the floodwater level z_i in the i-th flooded room is defined relative to Figure 3. In the case of a fully flooded room, the water level can be replaced by the water head ζ_i measured in meters, which represents the pressure inside the filled room.

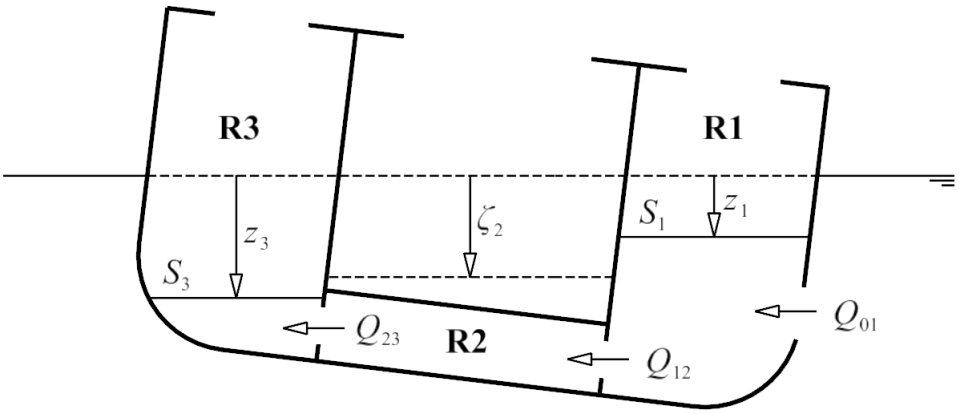

Figure 3. Illustration of a simple three-room geometry [31].

In this framework, the governing equations describing the progressive flooding process involve mass conservation for each room and momentum conservation for all openings connecting two rooms or a room to the sea. The steady Bernoulli equation is commonly applied to model the latter [35]. For the i-th room, connected to other rooms by N_i deeply submerged openings, the governing equations are expressed as follows [36]:

$$\dot{z}_i \mu_i S_i \approx \dot{V}_i = \sum_{j=1}^{N_i} Q_{ji} \tag{2a}$$

$$Q_{ji} = C_{d_{ji}} A_{ji} \mathrm{sgn}(z_j - z_i) \sqrt{2g|z_j - z_i|} \tag{2b}$$

where Q_{ji} denotes the volumetric flow rate through an opening connecting the j-th to i-th rooms, A_{ji} represents its gross area, $C_{d_{ji}}$ is the discharge coefficient to model its pressure drop, $\dot{V}_i$ is the time derivative of floodwater volume within the i-th room, S_i denotes its free surface area, μ_i is its permeability, and g signifies the acceleration due to gravity. It is noteworthy that, for fully flooded rooms, in Equation (2a), the left-hand side is zero, and in Equation (2b), z_i is replaced by ζ_i.

2.4. Free Outflow Correction

As previously mentioned, all openings are assumed to be affected by deeply submerged flow. Therefore, this assumption cannot accurately model free outflow scenarios,

which are common in real ship environments. For large openings, various submersion statuses can be identified, as illustrated in Figure 4.

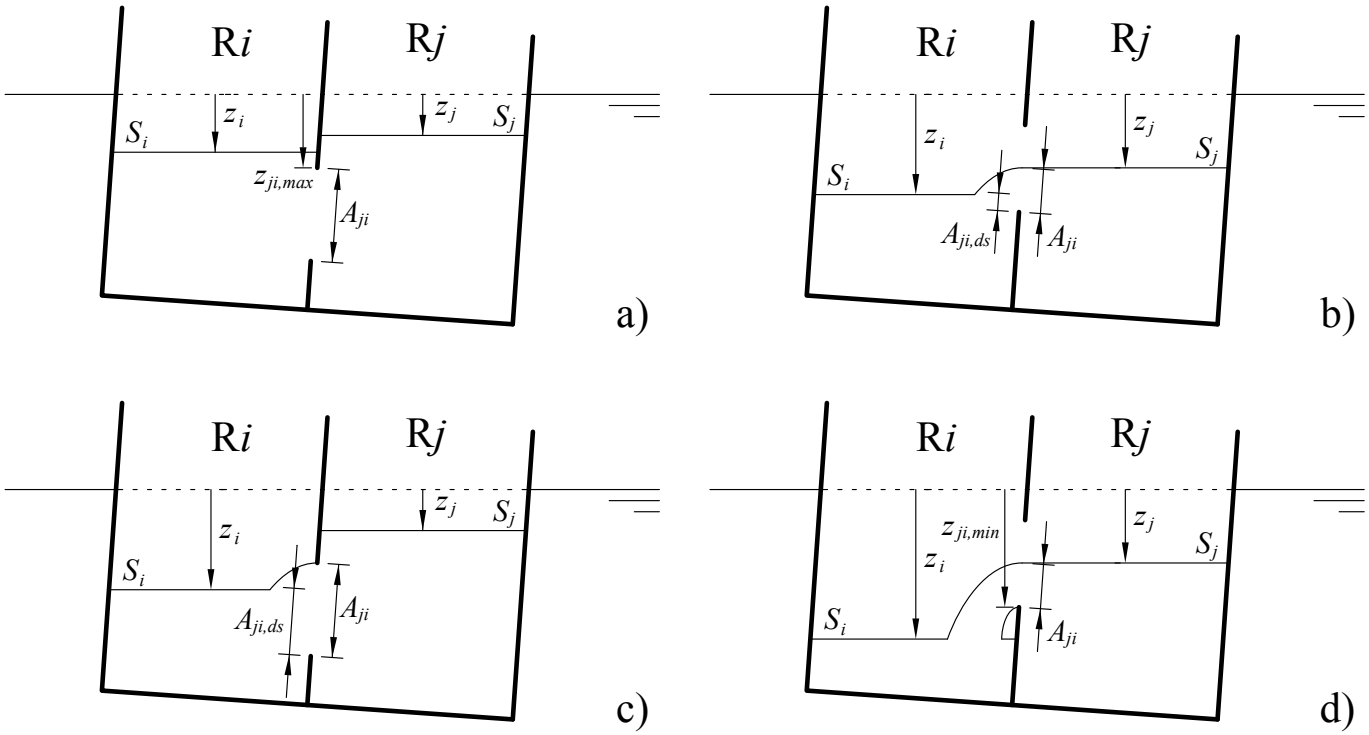

Figure 4. Sketch of different submersion statuses of a large opening: (**a**) deeply submerged; (**b**) free outflow with deeply submerged part; (**c**) deeply submerged one side only; (**d**) free outflow.

Equation (2b) models the flow rate for deeply submerged openings, where the conditions $z_{max_{ji}} < z_i$ and $z_{max_{ji}} < z_j$ are satisfied. In such cases, the deeply submerged area $A_{ds_{ji}}$ equals the opening area A_{ji}, as depicted in Figure 4a. Conversely, in scenarios like Figure 4d, the entire area A_{ji} is affected by free outflow. For other cases (Figure 4b,c), the free outflow area $A_{fo_{ji}}$ can be calculated as

$$A_{fo_{ji}} = A_{ji} - A_{ds_{ji}} \tag{3}$$

Considering a general case and assuming a flat rectangular opening (which is extremely common in ship subdivision [32] and in modelling damages [37]), the flow rate for free outflow is given by

$$Q_{fo_{ji}} = \int_{z_b}^{z_t} C_{d_{ji}} \frac{A_{fo_{ji}}}{z_t - z_b} \sqrt{2g(z_j - z)}\, \mathrm{d}z \tag{4}$$

where $z_b = \max(z_i, z_{min_{ji}})$ and $z_t = \min(z_j, z_{max_{ji}})$. Integrating Equation (4), the flow rate is given by

$$Q_{fo_{ji}} = C_{d_{ji}} \sqrt{2g} \frac{A_{fo_{ji}}}{z_t - z_b} \frac{2}{3} \left[(z_j - z_b)^{\frac{3}{2}} - (z_j - z_t)^{\frac{3}{2}} \right] \tag{5}$$

Introducing these equations directly into the governing equations (Equations (2a) and (2b)) to model free outflow would render the resulting system non-linearisable and analytically unsolvable, thereby forfeiting the computational efficiency advantages. To maintain linearisability and prevent errors arising from neglecting free outflow, the correct flow rate can be modelled using deeply submerged formulation as in Equation (2b), with a reduced effective area $A_{e_{ji}}$, as

$$Q_{fo_{ji}} = C_{d_{ji}} A_{e_{ji}} \sqrt{2g(z_j - z_b)} \tag{6}$$

Equating Equations (5) and (6), a correction factor γ_{ji} for the free outflow area can be defined as

$$\gamma_{ji} = \frac{A_{e_{ji}}}{A_{fo_{ji}}} = \frac{2}{3} \frac{\left[(z_j - z_b)^{\frac{3}{2}} - (z_j - z_t)^{\frac{3}{2}}\right]}{\sqrt{(z_j - z_b)}(z_t - z_b)} \tag{7}$$

This general equation can be applied to all the cases of free outflow. If $z_j \leq z_{max_{ji}}$, i.e., when the opening is only partially submerged by the floodwater level in the room having the highest level, Equation (7) can be further simplified to $\gamma_{ji_s} = 2/3$.

Therefore, to maintain the feasibility of linearization, the deeply submerged formulation in Equation (2b) can still be applied in all cases depicted in Figure 4, provided the opening area is adjusted according to

$$A_{ji} = A_{ds_{ji}} + \gamma_{ji} A_{fo_{ji}} \tag{8}$$

It is noteworthy that this formulation is not suitable for horizontal openings in the Earth-fixed reference system. In such cases, a unity correction factor should be applied to both upflooding and downflooding scenarios.

Finally, if the floodwater level in the room with the lower level is lower than the lowest tip of the opening, to avoid overestimating the flow rate, $\widetilde{z}_i$ should be used instead of z_i in Equation (2b)

$$\widetilde{z}_i = \begin{cases} z_{ij_{min}} & \text{if} \quad z_i < z_{ij_{min}} \\ z_i & \text{if} \quad z_i \geq z_{ij_{min}} \end{cases} \tag{9}$$

This adjustment models the outflow with an effective level difference of $z_j - z_{ij_{min}}$ instead of the overestimated $z_j - z_i$, which is implicit in governing Equation (2b).

2.5. System of Equations

Considering n partially flooded rooms and $m - n$ fully flooded rooms, to capture the behaviour in both room types during a time step dt of the integration process beginning at t^*, the floodwater levels evolution can be modelled through a non-linear semi-explicit Differential Algebraic Equation (DAE) system. Combining the Equations (2a) and (2b) while considering Equations (8) and (9), the system reads

$$\begin{cases} \dot{\mathbf{z}}(t - t^*) &= f(\mathbf{z}(t - t^*), \boldsymbol{\zeta}(t - t^*)) \\ \mathbf{0} &= g(\mathbf{z}(t - t^*), \boldsymbol{\zeta}(t - t^*)) \end{cases} \tag{10}$$

where the $\mathbf{z}$ values are still the floodwater levels inside the n partially filled rooms, while $\boldsymbol{\zeta}$ values are the water heads inside the $m - n$ completely filled ones, both expressed in the Earth-fixed reference system. The functions f and g can be written as

$$f_i(\mathbf{z}(t - t^*), \boldsymbol{\zeta}(t - t^*)) = \sum_{\substack{j=0 \\ j \neq i}}^{n} \frac{K_{ji}}{\mu_i S_i} \operatorname{sgn}(z_j - z_i) \sqrt{|z_j - z_i|} + \sum_{j=n+1}^{m} \frac{K_{ji}}{\mu_i S_i} \operatorname{sgn}(\zeta_j - z_i) \sqrt{|\zeta_j - z_i|} \tag{11a}$$

$$g_i(\mathbf{z}(t - t^*), \boldsymbol{\zeta}(t - t^*)) = \sum_{j=0}^{n} K_{ji} \operatorname{sgn}(z_j - \zeta_i) \sqrt{|z_j - \zeta_i|} + \sum_{\substack{j=n+1 \\ j \neq i}}^{m} K_{ji} \operatorname{sgn}(\zeta_j - \zeta_i) \sqrt{|\zeta_j - \zeta_i|} \tag{11b}$$

with the constant K_{ji} defined as

$$K_{ji} = C_{d_{ji}} A_{ji} \sqrt{2g} \tag{12}$$

2.6. Partially Flooded Rooms

The differential component of System (10) can be linearised to allow the derivation of an analytical solution for predicting the updated levels at the conclusion of the integration time step dt. By introducing a perturbation in levels, $\mathbf{z}' = \mathbf{z} - \mathbf{z}^*$, where $\mathbf{z}^* = \mathbf{z}(t^*)$

represents the initial levels, and the system's differential part can be linearised around $\mathbf{z}^*$ as follows:

$$\dot{\mathbf{z}}' = \mathbf{J}_f(\mathbf{z}^*, \boldsymbol{\zeta}^*)\mathbf{z}' + f(\mathbf{z}^*, \boldsymbol{\zeta}^*) \tag{13}$$

where $\mathbf{J}_f$ denotes the Jacobian matrix of the function f evaluated at $(\mathbf{z}^*, \boldsymbol{\zeta}^*)$, with elements defined as

$$J_{f_{ij}} = \begin{cases} -\sum\limits_{\substack{k=0 \\ k\neq i}}^{n} \dfrac{K_{ki}}{S_i\mu_i\sqrt{|z_k^* - z_i^*|}} - \sum\limits_{k=n+1}^{m} \dfrac{K_{ki}}{S_i\mu_i\sqrt{|\zeta_k^* - z_i^*|}} & \text{if} \quad i = j \\ \dfrac{K_{ji}}{S_i\mu_i\sqrt{|z_j^* - z_i^*|}} & \text{if} \quad i \neq j \end{cases} \tag{14}$$

According to [31], the Jacobian matrix is diagonalisable. Hence, it can be decomposed through the single value decomposition as

$$\mathbf{J}_f(\mathbf{z}^*, \boldsymbol{\zeta}^*) = \mathbf{V} \times \mathbf{D} \times \mathbf{V}^{-1} \tag{15}$$

where $\mathbf{D}$ is a diagonal matrix. Introducing $\mathbf{u} = \mathbf{V}^{-1}\mathbf{z}'$, the Equation (10) can be rewritten as

$$\dot{\mathbf{u}} = \mathbf{D}\mathbf{u} + \mathbf{v} \tag{16}$$

where

$$\mathbf{v} = \mathbf{V}^{-1} f(\mathbf{z}^*, \boldsymbol{\zeta}^*) \tag{17}$$

The differential equations of the System (16) are decoupled. Therefore, an algebraic solution can be obtained:

$$z_i = z_i^* + \sum_{j=1}^{n} \frac{V_{ij}v_j\left(e^{D_{jj}(t-t^*)} - 1\right)}{D_{jj}} \tag{18}$$

2.7. Fully Flooded Rooms

Once the time step dt is defined, the algebraic solution yields the next iteration levels $\mathbf{z}(\mathrm{d}t)$. Subsequently, the water head in completely filled rooms can be determined by solving the algebraic part of System (10) in $\boldsymbol{\zeta}(t)$. This system is non-linear and differentiable, with its Jacobian matrix $\mathbf{J}_g$ given by:

$$J_{g_{ij}} = \begin{cases} -\sum\limits_{k=0}^{n} \dfrac{K_{ki}}{\sqrt{4|z_k(\mathrm{d}t) - \zeta_i|}} - \sum\limits_{\substack{k=n+1 \\ k\neq i}}^{m} \dfrac{K_{ki}}{\sqrt{4|\zeta_k - \zeta_i|}} & \text{if} \quad i = j \\ \dfrac{K_{ji}}{\sqrt{4|\zeta_j - \zeta_i|}} & \text{if} \quad i \neq j \end{cases} \tag{19}$$

As a result, the system is approached as a least-squares problem. This study utilizes the Levenberg–Marquardt algorithm, initializing with $\boldsymbol{\zeta}^* = \boldsymbol{\zeta}(t^*)$. The water heads that achieve the minimal condition are considered the system's solution $\boldsymbol{\zeta}(\mathrm{d}t)$, thereby defining the unknown variables for the next main-loop iteration. This approach allows for the independent modelling of each fully filled room, eliminating the need for grouping fully flooded rooms, as previously introduced by [31]. The earlier method neglected the pressure drop at major openings driving the grouping procedure, although it was not always negligible. In the current formulation, grouping is applied solely for level equalization when the pressure drop is actually negligible.

2.8. Adaptive Time Step

The progressive flooding process is characterized by varying rates of evolution. During transient events, the process evolves rapidly, then slows down, approximating a decaying exponential trend as described by Equation (18). However, sudden accelerations can occur due to the collapse of a non-watertight door, the sudden immersion of a large opening, or the onset of capsizing. Thus, applying a constant integration step is impractical as it would be calibrated for the slowest phase, thereby increasing computational effort for all other phases [31]. Therefore, in this study, the time step is updated at each iteration through an adaptive procedure based on the derivatives of floodwater levels, $\dot{\mathbf{z}}^*$, computed at t^* using Equation (11a):

$$\mathrm{d}t = k_{\mathrm{d}t} \frac{z_b}{\max \dot{\mathbf{z}}^*} \tag{20}$$

where $k_{\mathrm{d}t}$ is a constant that governs integration accuracy. A reference value of $k_{\mathrm{d}t}$ is set to 0.01, based on the experimental tuning conducted in [31].

Although adaptive time steps can reduce computation time, excessively large time steps may compromise simulation accuracy due to

- The delayed detection of the submersion of a PFO and the subsequent addition of a new flooded room.
- The late identification of room-filling, delaying the transition from the differential to the analytical formulation.
- Significant changes in the ship's floating position, conflicting with the assumption of a fixed floating position over a single time step.

All these problems could be mitigated by defining a maximum time step $\mathrm{d}t_{\max}$ a priori, based on the results of the latest integration steps. Using an exponential fitting of the last two steps, the maximum time step related to a critical event e can be defined as follows:

$$\mathrm{d}t_e = \left[\frac{\ln\left(\frac{x_e}{x^{**}}\right)}{\ln\left(\frac{x^*}{x^{**}}\right)} - 1 \right] \mathrm{d}t^* \tag{21}$$

where x is a quantity used to identify event occurrence; x_e is its critical value associated with event occurrence; $\mathrm{d}t^*$ and $x^* = x(t^*)$ are the last time step and the last value of the critical quantity, respectively; and $x^{**} = x(t^* - \mathrm{d}t^*)$ is the penultimate value of x. Table 2 provides descriptions and critical values for all the quantities monitored for evaluating the maximum time step.

Table 2. Quantities and reference values for the assessment of maximum time step.

Description	Quantity x	Critical Value x_e
Submersion of PFO in i-th room	z_i	Level of lower tip of the PFO z_{PFO}
Filling of i-th room	z_i	Maximum level of the room z_{max_i}
Excessive change in heel angle	$\lvert\Delta\phi\rvert$	0.100 deg
Excessive change in trim angle	$\lvert\Delta\theta\rvert$	0.050 deg
Excessive change in non-dimensional mean draught	$\lvert\Delta T_M\rvert/(T_{M_0})$	0.005

3. Validation of Free Outflow Correction

This section validates the new method for addressing free outflow scenarios using the linearised simulation technique by comparing it with experimental data. Model-scale experiments on a box-shaped barge conducted at MARIN provide the basis for this comparison [35]. The experimental setup and corresponding results are presented hereinafter.

3.1. Experimental Set-Up

The selected geometry consists of a box-shaped model divided into two compartments by a deck, as depicted in Figure 5. Both compartments are fully vented, with the lower compartment (C1) connected to the upper compartment (C2) through a rectangular opening.

Upflooding and downflooding tests were performed on the barge under fixed heel, trim, and draught conditions, with two potential breaches connecting the internal compartments to the sea. This study specifically addresses the downflooding scenario, which presents significant modelling challenges. Consequently, only the Sea-C2 breach was considered open during the simulations.

A non-structured triangular mesh was used to model the box and internal openings, enabling volume calculations via an in-house code based on pressure integration [34]. The code splits the mesh panels at the free surface intersection for both hull and rooms to fully capture the shape of the submerged body. Careful attention was given to replicating the deck thickness and the vent pipe of compartment C1, resulting in the meshes illustrated in Figure 6. The maximum panel size has been set to 0.001 m^2.

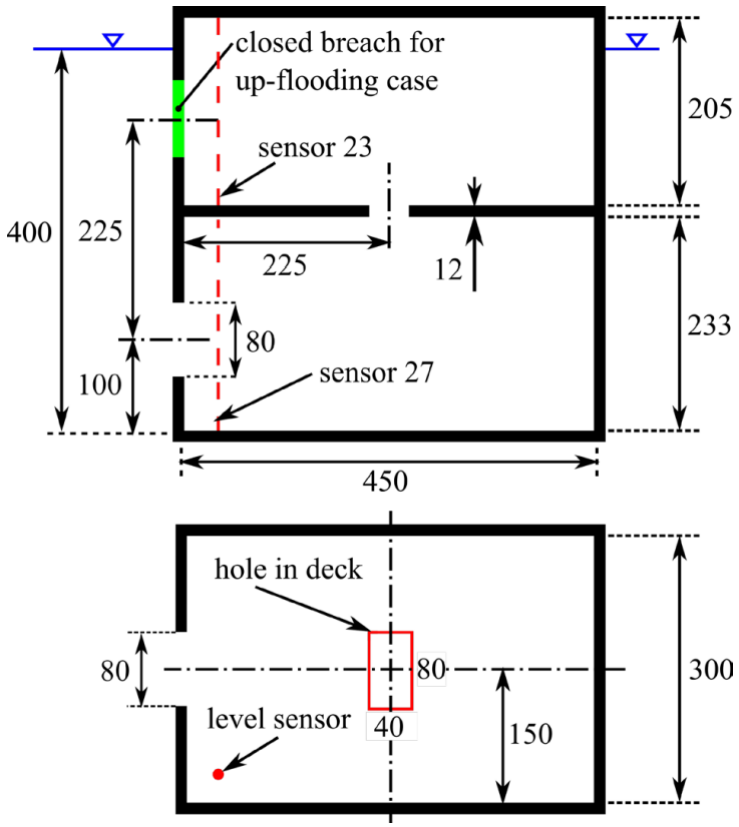

Figure 5. Experimental setup utilized [35]. All measurements are in mm. Floodwater levels in C1 and C2 were measured using level sensors 27 and 23, respectively.

This specific geometry was chosen because the fixed floating position allows the study of water flow through openings without interference from equilibrium position calculations.

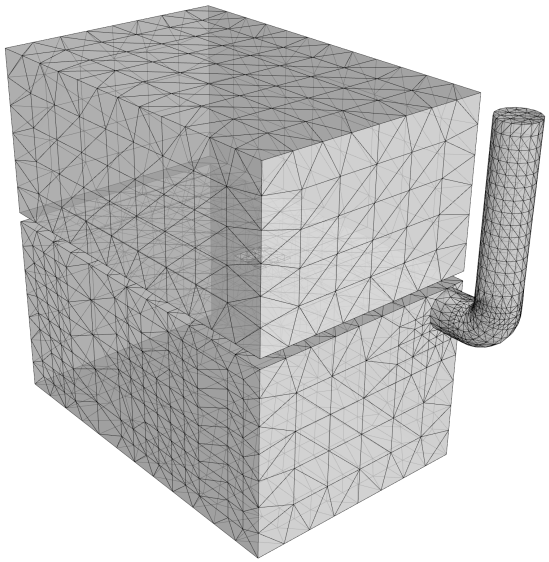

Figure 6. Mesh of the box-model used to simulate progressive flooding.

3.2. Results

Figures 7 and 8 depict the simulation results for the downflooding scenario in the test geometry. Figure 7 illustrates the temporal evolution of water levels in compartment C1, while Figure 8 shows the corresponding levels in compartment C2, which is connected to open water. The simulations were conducted using two methods:

- One using solely the deeply submerged formulation according to govering equations given in Section 2.3;
- One with the incorporated correction for free outflow modelling presented in Section 2.4.

These results are compared with experimental measurements conducted by MARIN.

The application of the deeply submerged formulation yields inaccurate results for the test case. Conversely, incorporating the correction to account for free outflow demonstrates a perfect match with the experimental results in this challenging scenario, thereby validating this approach.

In terms of computational effort, both formulations are entirely comparable. In the analysed test case, the corrected simulation is approximately 5% quicker than the deeply submerged one, primarily because the corrected formulation permits the use of larger time steps, due to its slower pace.

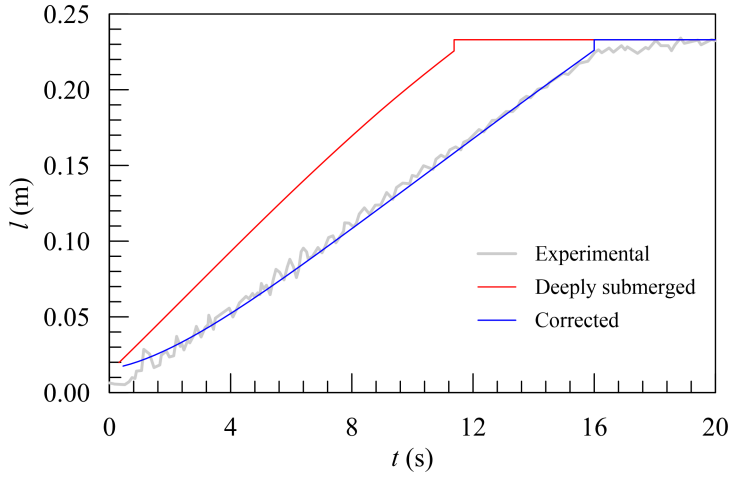

Figure 7. Simulated and experimental water levels in compartment C1.

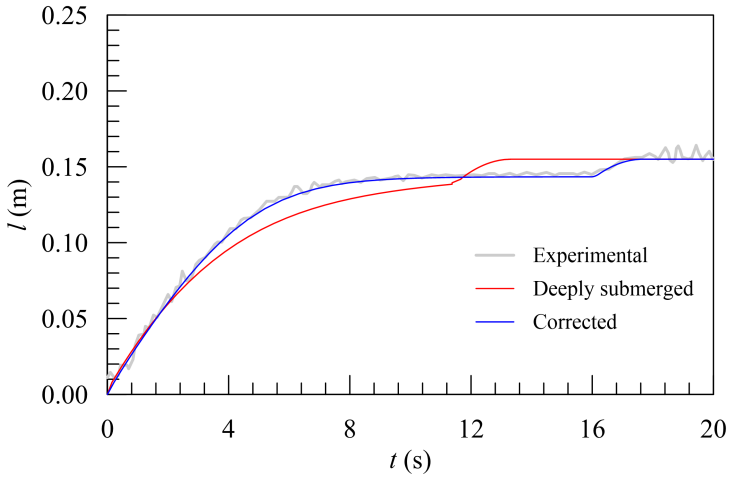

Figure 8. Simulated and experimental water levels in compartment C2.

4. Application

This section presents an application of the consolidated linearised method on a more complex scenario involving a cruise ship. Model scale experiments on a large passenger ships model with complex internal subdivisions were conducted at MARIN, providing the basis for this comparison [38]. The experimental setup and corresponding results are presented hereinafter.

4.1. Experimental Set-Up

The selected geometry consists of a large passenger ship model, whose main dimensions are reported in Table 3. Three compartments are modelled in high detail as well as four decks over the bulkhead deck, as depicted in Figure 9. All the rooms are fully vented and are connected by open openings with the shape and dimensions of standard fire and joiner doors installed on a cruise ship. In this study, the focus is on a scenario characterised by a large side breach, highlighted in red in Figure 9 leading to a very fast inflow of floodwater.

Table 3. Main particulars and initial floating position of the test ship.

Quantity	Symbol	Full Scale	Model Scale
Length overall	L_{OA}	300 m	5 m
Length between perpendiculars	L_{BP}	270 m	4.5 m
Breadth	B	35.2 m	0.587 m
Depth at bulkhead deck	D	11 m	0.183 m
Initial draught	T_{M_0}	8.2 m	0.137 m
Initial Trim	θ_0	0 deg	0 deg
initial Heel	ϕ_0	0 deg	0 deg
Initial metacentric heigh	GM_0	2.36 m	0.0393 m

Again, non-structured triangular meshes were used to model the ship hull, subdivision and internal openings. The maximum size of the panels were gradually reduced until the convergence of hydrostatics values was obtained [38] while for openings' meshes, previous standards for model-scale simulations were adopted, as in [31]. Careful attention was given to replicating the boundary thickness and additional subdivision of double bottom spaces in order to model cross-flooding, resulting in the meshes illustrated in Figure 10. Vent pipes were not modelled. More details on the tests and arrangement can be found in [38].

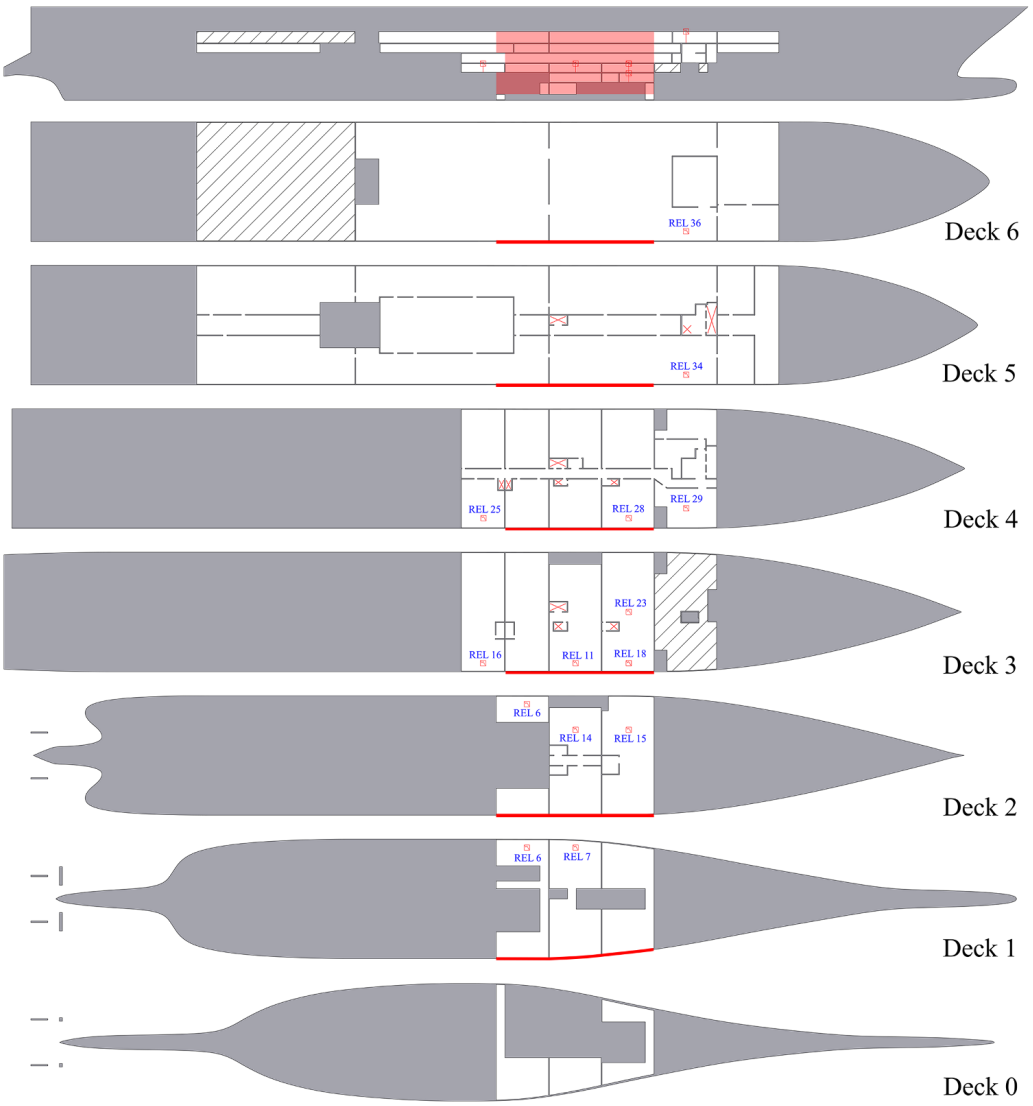

Figure 9. Experimental setup utilized [38]. All measurements are in mm. Floodwater levels in C1 and C2 were measured using level sensors 27 and 23, respectively.

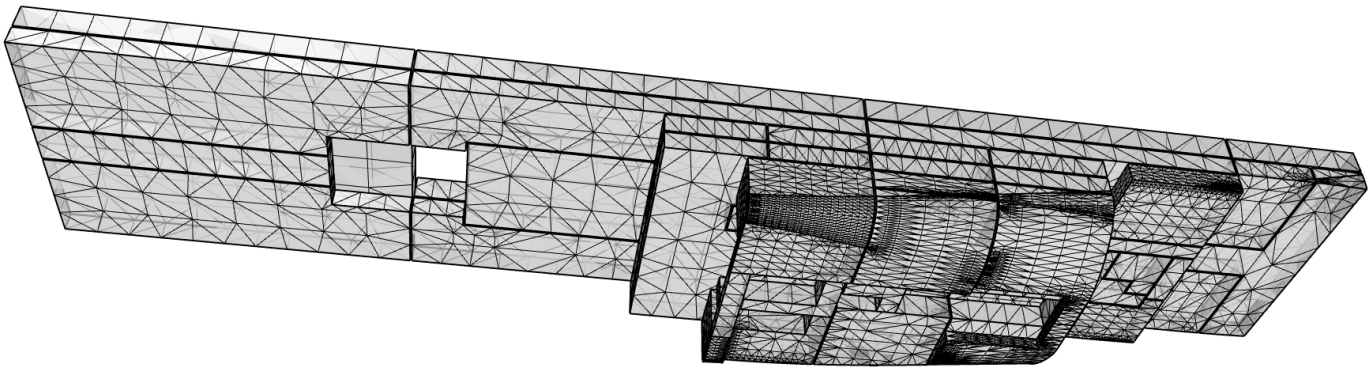

Figure 10. Mesh of the shop model rooms used for simulating progressive flooding

4.2. Results

Figure 11 presents the time records for heel, trim, and water level, obtained from several relevant sensors: REL 6 on Deck 1 (port side), REL 14 on Deck 2 (port side), REL 28

on Deck 4 (starboard side), and REL 34 on Deck 5 (starboard side). The simulation required 336 s of computational time.

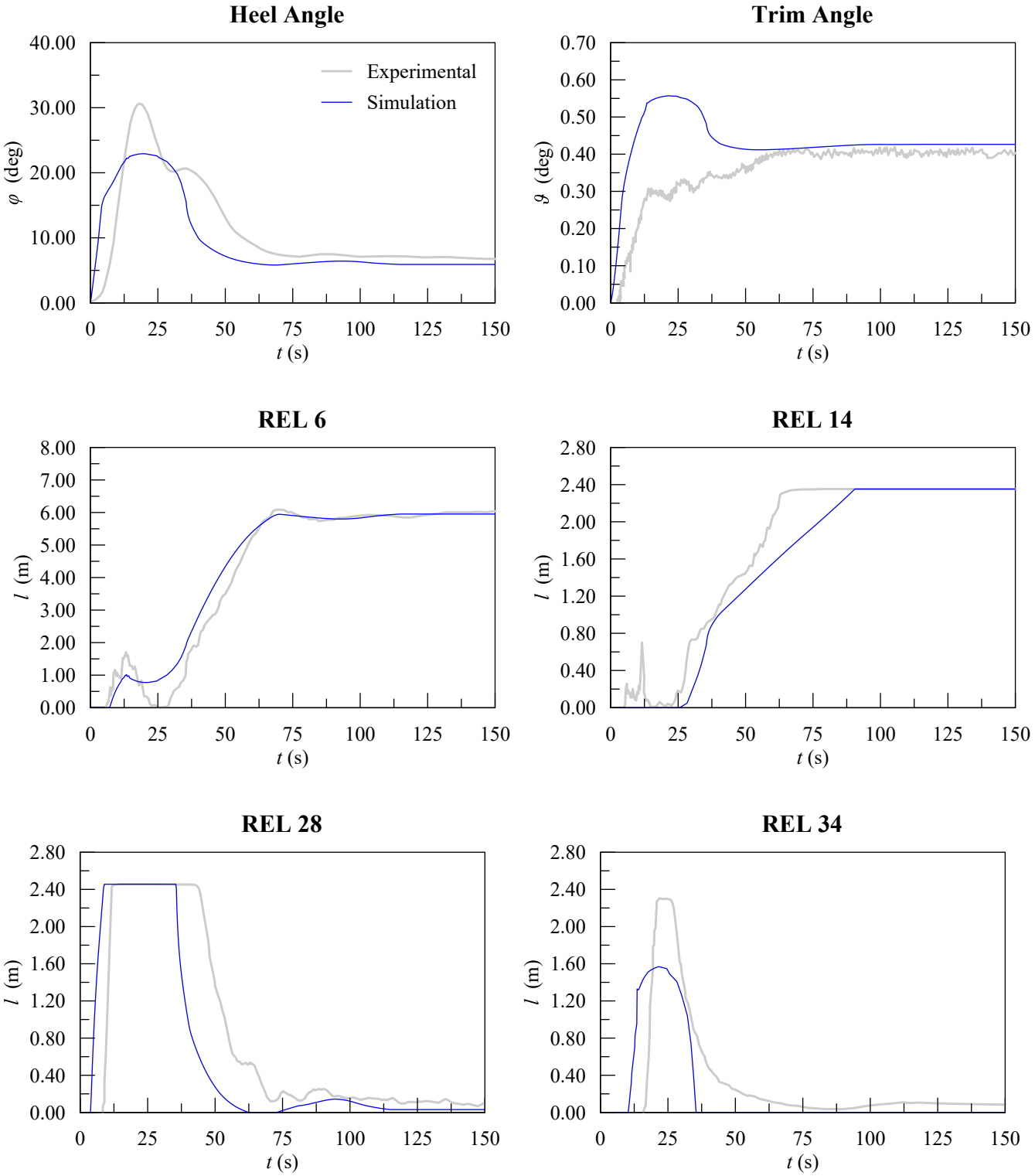

Figure 11. Comparison of the experimental and simulated heel, trim, and levels recorded by sensors for the ship model

At the beginning of the experiment, extensive damage resulted in a dynamic transient phase that a quasi-static simulation cannot fully replicate. Consequently, the simulation underestimated the maximum roll angle by approximately 7 deg and oscillations were

absent. A peak in the trim angle appeared in the simulation but was not observed during experimental tests. Eventually, the simulation accurately converged to the actual heel and trim angles at the end of the progressive flooding phase.

The simulation accurately predicted the water level recorded by sensor REL 6, but due to the lack of dynamic roll oscillations, the sensor did not dry up at $t \approx 20$ s. Similarly, the simulation failed to capture the initial peak observed by sensor REL 14 before $t \approx 20$ s; however, it did correctly simulate subsequent phases, albeit with a slightly faster rise in water level. On Deck 4, the simulation accurately captured the initial flooding but anticipated the subsequent reduction in water level by approximately 10 s. On Deck 5, the maximum water level recorded by sensor REL 34 was underestimated, and the sensor dried up earlier than what was observed experimentally. The primary reason for these discrepancies is again the underestimation of the roll angle.

5. Discussion

Concerning the validation case, the implementation of the deeply submerged formulation results in a substantial overestimation of flow rates at model openings, particularly those located on the deck. By not considering the minimum height of the lowest point of the opening, the effective waterhead is calculated as the difference between the levels in compartments C2 and C1, causing a more rapid increase in floodwater level in C2 compared to experimental data.

Moreover, the water flow through the breach is also overestimated without applying the free outflow correction. In reality, the flow rate through the breach most frequently falls into conditions (d) or (c) as shown in Figure 4. However, due to the significant overestimation at the downflooding opening, the water level in C2 remains underestimated until C1 is completely filled.

Applying the free outflow correction and limiting the effective waterhead for the downflooding opening increases the time-to-flood by approximately 4 s, which represents 25% of the simulation time. Additionally, the corrected simulation matches the experimental records very closely, particularly in reproducing the water level in C2 with high accuracy. This indicates that the free outflow correction applied to the linearized method accurately captures the hydraulic flows governing the studied phenomena.

Moving to the ship model experiment, the chosen scenario presents a significant challenge for quasi-static code simulation, illustrating both the current strengths and areas for improvement. Specifically, it is clear that a quasi-static method, which relies on a fully static assessment of equilibrium floating position, is inadequate for handling dynamic transients caused by massive damage. Nevertheless, the method successfully captures the physical phenomena and time frame, aligning with results from fully dynamic and CFD codes as highlighted in the benchmark study that is deeply analysed in [38]. For example, most tested simulation methods failed to accurately capture the roll angle, and all of them showed a higher peak in the trim angle than those obtained by the linearised method.

These insights suggest the necessity of replacing the static equilibrium position with a one-degree-of-freedom dynamic model incorporating dynamic roll motion. Such an enhancement is expected to improve accuracy during transient flooding phases and potentially enable the introduction of the effects of regular and irregular waves into a fast simulation model that directly applicable onboard for decision support purposes.

It is noteworthy that even when a fast linearised simulation method was employed, the computational time for simulating the very large damage utilized in the ship model experiment was about three times longer than real-time in full scale. This implies that simulating massive damages remains challenging in an operational environment for decision support purposes. Nevertheless, scenarios with extremely rapid evolution (e.g., when the simulated scenario lasts 115 s in full scale) cannot be effectively addressed by an emergency DSS on a large passenger vessel, as evacuating the ship before the end of progressive flooding would be infeasible. This reduces the significance of the scenario as a benchmark for this kind of application. Considering a decision support purpose, these cases can be

handled only by DSS relying on pre-calculated damage scenarios or by employing machine learning [7,9]. In this context, it might be valuable to assess the accuracy improvement resulting from the introduction of the updated simulation method following the inclusion of free-outflow correction and dynamic roll.

A further critical issue in the experiments is the assumption that all openings are open to prevent or limit asymmetric flooding. The experiment demonstrates the effectiveness of this procedure, as evidenced by the rapid reduction in heel angle following the transient phase. However, this scenario is unlikely in real operational environments where fire and joiner doors are often closed, and requiring the crew to open them during progressive flooding could endanger their lives. Moreover, this contradicts the need to extend the time available in sink-or-capsize scenarios to facilitate ship evacuation [39]. These considerations must be properly considered and integrated into simulations driving an onboard DSS.

Finally, the ship model used in the simulations accurately represents the thickness of room boundaries and assumes unitary permeability, which does not accurately reflect the real internal spaces of passenger ships, as they are filled with machinery, piping, cabling, auxiliaries, and outfitting. The significant effect of permeability on progressive flooding has been previously demonstrated in [40,41] and warrants careful consideration to improve the accuracy of progressive flooding simulations in operational environments. Consequently, further research is necessary to ensure the precision and reliability of simulations used within onboard DSSs.

6. Conclusions

This research introduces a novel method for accurately simulating free outflow scenarios within linearised progressive flooding models. By embedding this approach into the main simulation loop, the method improves the calculation of subsequent floodwater levels, addressing inaccuracies stemming from the assumption of deeply submerged openings inherent in the original linearised techniques.

To validate the proposed approach, its performance was compared against experimental data using a simplified geometry. The results indicate that incorporating a correction factor for opening areas significantly enhances simulation accuracy, surpassing the original method based on deeply submerged openings. Furthermore, the study highlights the necessity of limiting effective waterheads in downflooding scenarios to prevent significant underestimations of the time to flood.

The addition of the free outflow correction broadens the scope of linearised techniques, making them applicable to a wider range of realistic progressive flooding scenarios in damaged ships. For the tested simple geometry, this enhancement in accuracy comes with no computational cost. Thus, its implementation can be recommended when a linearised simulation technique is employed, although further testing on complex geometries is still advisable. For instance, applying this technique to a large passenger ship model and comparing the experimental and simulated results yielded valuable insights for improving onboard DSS.

The ship model experiment has several scientific implications. First is the necessity to move beyond the quasi-static assumption for equilibrium assessment to effectively handle dynamic transients resulting from massive damage. Specifically, further research should incorporate dynamic roll motion into the floating position assessment of the linearised technique to enhance accuracy during transient flooding phases and integrate wave effects into fast simulation models for onboard DSSs. In addition, although the proposed method provided good results for cruise ships in both the model- and full-scale scenarios, it has not yet been tested on other ship types, which might require extra care in the modelling of roll dynamics and sloshing during the progressive flooding (e.g., RoRo ships, or cargo vessels having large holds).

Moreover, the computational time required to simulate massive damage scenarios remains a significant challenge for real-time decision support, highlighting the need for continued research to optimize these methods. Nonetheless, it is noteworthy that scenarios

involving very rapid damage progression or transient inaccuracies offer limited utility for emergency DSS, as they cannot provide useful insights if there is insufficient time for countermeasures. Therefore, for benchmarking and validating the simulations intended for onboard application, model tests on large passenger ships with smaller breaches and longer progressive flooding phases are still necessary.

Additionally, the current model's representation of doors, room boundaries, and permeability does not accurately reflect the complex internal spaces of passenger ships. Future research should focus on enhancing the realism of operational condition assumptions to improve the accuracy and reliability of onboard DSS simulations.

Author Contributions: Conceptualization, L.B.; methodology, L.B., J.P.-O. and S.B.; software, L.B.; validation, L.B., S.B., J.P.-O. and V.B.; formal analysis, L.B., S.B. and J.P.-O.; investigation, L.B.; resources, J.P.-O. and S.B.; data curation, S.B. and V.B.; writing—original draft preparation, L.B.; writing—review and editing, S.B., J.P.-O., V.B. and L.B.; visualization, L.B.; supervision, J.P.-O.; project administration, J.P.-O.; funding acquisition, J.P.-O. All authors have read and agreed to the published version of the manuscript.

Funding: This work has been fully supported by the Croatian Science Foundation under the project HRZZ-IP-2022-10-2821.

Institutional Review Board Statement: Not applicable.

Informed Consent Statement: Not applicable.

Data Availability Statement: Data is contained within the article.

Conflicts of Interest: The authors declare no conflicts of interest.

Abbreviations

The following abbreviations are used in this manuscript:

3D	Three-dimensional
CFD	Computational Fluid Dynamics
DAE	Differential Algebraic Equations
DSS	Decision Support System
MARIN	Maritime Research Institute Netherlands
PFO	Progressive Flooding Opening

References

1. Rodrigues, J.M. A Review of Methods for Modelling Flooding, Its Progression and Outcome in Damaged Ships. *J. Mar. Sci. Eng.* **2024**, *12*, 251. [CrossRef]
2. Dankowski, H.; Russel, P.; Krüger, S. New Insights Into the Flooding Sequence of the Costa Concordia Accident. In Proceedings of the 33rd International Conference on Ocean, Offshore and Arctic Engineering-OMAE 2014, San Francisco, CA, USA, 8–13 June 2014.
3. Ruponen, P.; Pennanen, P.; Manderbacka, T. On the alternative approaches to stability analysisin decision support for damaged passenger ships. *WMU J. Marit. Aff.* **2019**, *18*, 477–494. [CrossRef]
4. Penttilä, P.; Ruponen, P. Use of Level Sensors in Breach Estimation for a Damaged Ship. In Proceedings of the 5th International Conference on Collision and Grounding of Ships, Espoo, Finland, 14–16 July 2010; pp. 80–87.
5. Ruponen, P.; Lindroth, D.; Pennanen, P. Prediction of survivability for decision support in ship flooding emergency. In Proceedings of the 12th International Conference on the Stability of Ships and Ocean Vehicles, Glasgow, UK, 14–19 June 2015.
6. Lee, D.; Kim, S.; Lee, K.; Shin, S.c.; Choi, J.; Park, B.J.; Kang, H.J. Performance-based on-board damage control system for ships. *Ocean Eng.* **2021**, *223*, 108636. [CrossRef]
7. Braidotti, L.; Valčić, M.; Prpić-Oršić, J. Exploring a Flooding-Sensors-Agnostic Prediction of the Damage Consequences Based on Machine Learning. *J. Mar. Sci. Eng.* **2021**, *9*, 271. [CrossRef]
8. Son, H.y.; Roh, H.d.; Kim, G.y.; Oh, S.j.; Choi, J.; Lee, D.k.; Shin, S.c. Prediction of Flooded Compartment Damage Locations in Ships by Using Spectrum Analysis of Ship Motions in Waves. *J. Mar. Sci. Eng.* **2022**, *10*, 17. [CrossRef]
9. Son, H.y.; Kim, G.y.; Kang, H.j.; Choi, J.; Lee, D.k.; Shin, S.c. Ship Motion-Based Prediction of Damage Locations Using Bidirectional Long Short-Term Memory. *J. Ocean Eng. Technol.* **2022**, *36*, 295–302. [CrossRef]
10. Mauro, F.; Conti, F.; Vassalos, D. Damage surrogate models for real-time flooding risk assessment of passenger ships. *Ocean Eng.* **2023**, *285*, 115493. [CrossRef]

11. Louvros, P.; Stefanidis, F.; Boulougouris, E.; Komianos, A.; Vassalos, D. Machine Learning and Case-Based Reasoning for Real-Time Onboard Prediction of the Survivability of Ships. *J. Mar. Sci. Eng.* **2023**, *11*, 890. [CrossRef]
12. Manderbacka, T.; Mikkola, T.; Ruponen, P.; Matusiak, J. Transient response of a ship to an abrupt flooding accounting for the momentum flux. *J. Fluids Struct.* **2015**, *57*, 108–126. [CrossRef]
13. Acanfora, M.; Begovic, E.; De Luca, F. A Fast Simulation Method for Damaged Ship Dynamics. *J. Mar. Sci. Eng.* **2019**, *7*, 111. [CrossRef]
14. Hashimoto, H.; Kawamura, K.; Sueyoshi, M. A numerical simulation method for transient behavior of damaged ships associated with flooding. *Ocean Eng.* **2017**, *143*, 282–294. [CrossRef]
15. Caldas, A.; Zegos, C.; Skoupas, S.; Jenkins, J. Ship survivability study using high fidelity CFD. In Proceedings of the 19th International Conference on Ships and Maritime Research-NAV, Trieste, Italy, 20–22 June 2018;
16. Zhang, X.; Lin, Z.; Li, P.; Dong, Y.; Liu, F. Time Domain Simulation of Damage Flooding Considering Air Compression Characteristics. *Water* **2019**, *11*, 796. [CrossRef]
17. Spouge, J. Technical Investigation of the Sinking of the Ro-Ro Ferry European Gateway. *Trans. RINA* **1986**, *128*, 49–72.
18. de Kat, J. Dynamics of a ship with partially flooded compartment. In *Contemporary Ideas on Ship Stability*; Vassalos, D., Hamamoto, M., Papanikolaou, A., Molyneux, D., Eds.; Elsevier Science: Amsterdam, The Netherlands, 2000.
19. Santos, T.; Winkle, I.; Guedes Soares, C. Time domain modelling of the transient asymmetric flooding of Ro-Ro ships. *Ocean Eng.* **2002**, *29*, 667–688. [CrossRef]
20. Ruponen, P. Progressive Flooding of a Damaged Passenger Ship. Ph.D. Thesis, Helsinki University of Technology, Helsinki, Finland, 2007.
21. Ruponen, P.; Sundell, T.; Larmela, M. Validation of a simulation method for progressive flooding. *Int. Shipbuild. Prog.* **2007**, *54*, 305–321.
22. Ruponen, P.; Kurvinen, P.; Saisto, I.; Harras, J. Experimental and Numerical Study on Progressive Flooding in Full-Scale. *Int. J. Marit. Eng.* **2010**, *152*, 197–208. [CrossRef]
23. Dankowski, H.; Krüger, S. A Fast, Direct Approach for the Simulation of Damage Scenarios in the Time Domain. In Proceedings of the 11th International Marine Design Conference-IMDC 2012, Glasgow, UK, 11–14 June 2012.
24. Dankowski, H. A Fast and Explicit Method for Simulating Flooding and Sinkage Scenarios of Ships. Ph.D Thesis, Technischen Universität Hamburg, Hamburg, Germany, 2013.
25. Rodrigues, J.; Guedes Soares, C. A generalized adaptive mesh pressure integration technique applied to progressive flooding of floating bodies in still water. *Ocean Eng.* **2015**, *110*, 140–151. [CrossRef]
26. Lee, G. A study on the dynamic orifice equation for the flooding simulation of a ship. *J. Ships Ocean Eng.* **2014**, *55*, 17–27.
27. Lee, G. Dynamic orifice flow model and compartment models for flooding simulation of a damaged ship. *Ocean Eng.* **2015**, *109*, 635–653. [CrossRef]
28. Ruponen, P.; Larmela, M.; Pennanen, P. Flooding Prediction Onboard a Damage Ship. In Proceedings of the 11th International Conference on the Stability of Ships and Ocean Vehicles, Athens, Grece, 23–28 September 2012; pp. 391–400.
29. Ruponen, P.; Pulkkinen, A.; Laaksonen, J. A method for breach assessment onboard a damaged passenger ship. *Appl. Ocean Res.* **2017**, *64*, 236–248. [CrossRef]
30. Ruponen, P. Adaptive time step in simulation of progressive flooding. *Ocean Eng.* **2014**, *78*, 35–44. [CrossRef]
31. Braidotti, L.; Mauro, F. A Fast Algorithm for Onboard Progressive Flooding Simulation. *J. Marit. Sci. Eng.* **2020**, *8*, 369. [CrossRef]
32. Braidotti, L.; Degan, G.; Bertagna, S.; Bucci, V.; Marinò, A. A Comparison of Different Linearized Formulations for Progressive Flooding Simulations in Full-Scale. *Procedia Comput. Sci.* **2021**, *180*, 219–228. [CrossRef]
33. Rodrigues, J.; Lavrov, A.; Hinostroza, M.; Guedes Soares, C. Experimental and numerical investigation of the partial flooding of a barge model. *Ocean Eng.* **2018**, *169*, 586–603. [CrossRef]
34. Braidotti, L.; Trincas, G.; Bucci, V. Analysis of the Influence of Pressure Field on Accuracy for Onboard Stability Codes. In Proceedings of the 19th International Conference on Ships and Maritime Research-NAV 2018, Trieste, Italy, 20–22 June 2018; pp. 80–87. [CrossRef]
35. Ruponen, P.; van Basten Batenburg, R.; Bandringa, H.; Braidotti, L.; Bu, S.; Dankowski, H.; Lee, G.; Mauro, F.; Murphy, A.; Rosano, G.; et al. Benchmark Study on Simulation of Flooding Progression. In Proceedings of the 1st International Conference on the Stability and Safety of Ships and Ocean Vehicles, Glasgow, UK, 7–11 June 2021.
36. Ruponen, P. Pressure-Correction Method for Simulation of Progressive Flooding and Internal Air flows. *Ship Technol. Res.* **2006**, *53*, 63–73. [CrossRef]
37. Ruponen, P.; Lindroth, D.; Routi, A.; Aartovaara, M. Simulation-based analysis method for damage survivability of passenger ships. *Ship Technol. Res.* **2019**, *66*, 180–192. [CrossRef]
38. Ruponen, P.; van Basten Batenburg, R.; van't Veer, R.; Braidotti, L.; Bu, S.; Dankowski, H.; Lee, G.J.; Mauro, F.; Ruth, E.; Tompuri, M. International benchmark study on numerical simulation of flooding and motions of a damaged cruise ship. *Appl. Ocean Res.* **2022**, *129*, 103403. [CrossRef]
39. Ruponen, P. On the effects of non-watertight doors on progressive flooding in a damaged passenger ship. *Ocean Eng.* **2017**, *130*, 115–125. [CrossRef]

40. Vassalos, D.; Paterson, D.; Mauro, F.; Atzampos, G.; Assinder, P.; Janicek, A. High-Expansion Foam: A Risk Control Option to Increase Passenger Ship Safety during Flooding. *Appl. Sci.* **2022**, *12*, 4949. [CrossRef]
41. Vassalos, D.; Atzampos, G.; Paterson, D.; Mauro, F. Permeable Volume—The Forgotten "Galaxy" in Ship Design. In Proceedings of the SNAME 14th International Marine Design Conference, Vancouver, BC, Canada, 26–30 June 2022. [CrossRef]